Supporting Information

Anionic Redox Reactions and Structural Degradation in a Cation-Disordered Rock-Salt $Li_{1.2}Ti_{0.4}Mn_{0.4}O_2$ Cathode Material Revealed by Solid-State NMR and EPR

Fushan Geng,[a] Bei Hu,[a] Chao Li,[a] Chong Zhao,[a] Olivier Lafon,[b,c] Julien Trébosc,[b,d] Jean-Paul Amoureux,[b,e,f] Ming Shen,[a] and Bingwen Hu[*a]*

[a] Shanghai Key Laboratory of Magnetic Resonance, State Key Laboratory of Precision Spectroscopy, School of Physics and Electronic Science, East China Normal University, Shanghai 200062, P.R. China.

[b] Univ. Lille, CNRS, Centrale Lille, Univ. Artois, UMR 8181, UCCS – Unité de Catalyse et de Chimie du Solide, F-59000 Lille, France.

[c] Institut Universitaire de France, 1 rue Descartes, F-75231 Paris, France.

[d] Univ. Lille, CNRS-2638, Fédération Chevreul, F-59000 Lille, France.

[e] Bruker Biospin, 34 rue de l'industrie, F-67166 Wissembourg, France.

[f] Riken NMR Science and Development Division, Yokohama, 230-0045 Kanagawa, Japan.

Corresponding Author: (B.H.) bwhu@phy.ecnu.edu.cn

Paramagnetic environments for Li in the $Li_{1.2}Ti_{0.4}Mn_{0.4}O_2$

According to the theory on the transfer of hyperfine interaction,[1] the unpaired electron spin density is transferred to the Li site in rock-salt structure through Li–O–Mn bonds with bond angles of 90° or 180°. In LTMO, a given Li atom has 12 nearest-neighbor cations with bond angles of 90° and 6 next-nearest cations with bond angles of 180°. The differences in paramagnetic shifts are only related to the populations of Mn^{3+} ions with Li–O–Mn bond angles of 90° and 180° since the diamagnetic Li^+ and Ti^{4+} cations do not produce Fermi contact shift. The number of Mn^{3+} ions in 90° interaction can vary from 0 to 12, i.e., 13 different configurations, whereas the number of Mn^{3+} ions can range from 0 to 6, i.e., 7 different configurations. Hence, there is a priori at least $7\times13-1 = 90$ possible configurations around the ^{7}Li nuclei resulting in different paramagnetic shifts. The population of each configuration is unknown, since it depends on the synthesis condition.

Weighted average shifts of the ^{7}Li NMR spectra

Assuming that there are *i* types of Li environments, each environment corresponds to a shift δ_i, and the population of each environment is P_i, the total population is the sum of the population of each environment, $P = \sum_i P_i$. The population P_i can be regarded as the weight of each shift. Now we use the weighted average shift δ_{wa} to evaluate the magnitude of the shifts. Assuming the NMR signal intensity $S(\delta)$ is proportional to the population P_i, the weighted average shift δ_{wa} is calculated as follow:

$$\delta_{wa} = \frac{\sum_i P_i \cdot \delta_i}{\sum_i P_i} = \frac{\int S(\delta) \cdot \delta d\delta}{\int S(\delta) d\delta}$$

The variation in the ^{7}Li NMR spectra results from two effects: the change in the Li contents and the change of local magnetism. These two kinds of changes are associated to changes in the population. If the Li atoms in diamagnetic environment are extracted from the material, δ_{wa} increases. If the local magnetism increases, δ_{wa} increases. At the last stage of charging, the

proportion of Li in paramagnetic environment is 95.7%. Thus, in that state of charge, the variation in the paramagnetic environment is more precisely detected using the weighted average shifts than the shift of the deconvoluted signal of Li in paramagnetic environment.

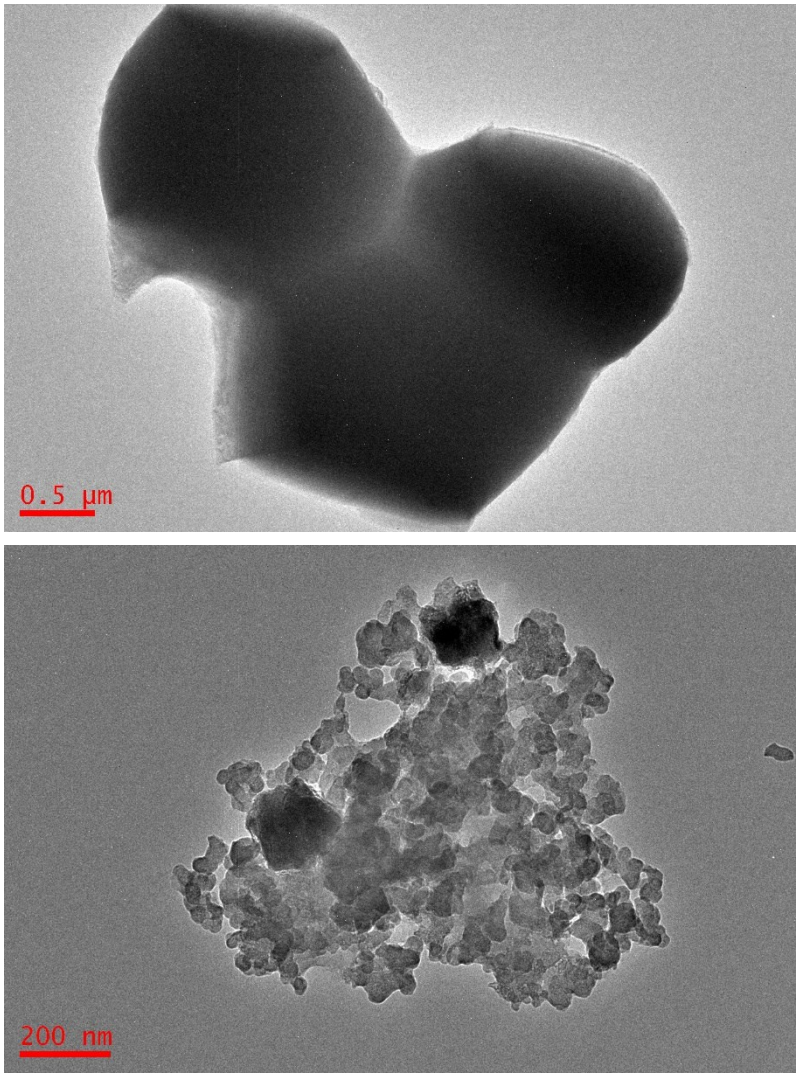

Figure S1. TEM images of the pristine (top) and the ball-milled (bottom) $Li_{1.2}Ti_{0.4}Mn_{0.4}O_2$. The aggregation of the light-colored particles in the ball-milled consists of the Super P carbon black.

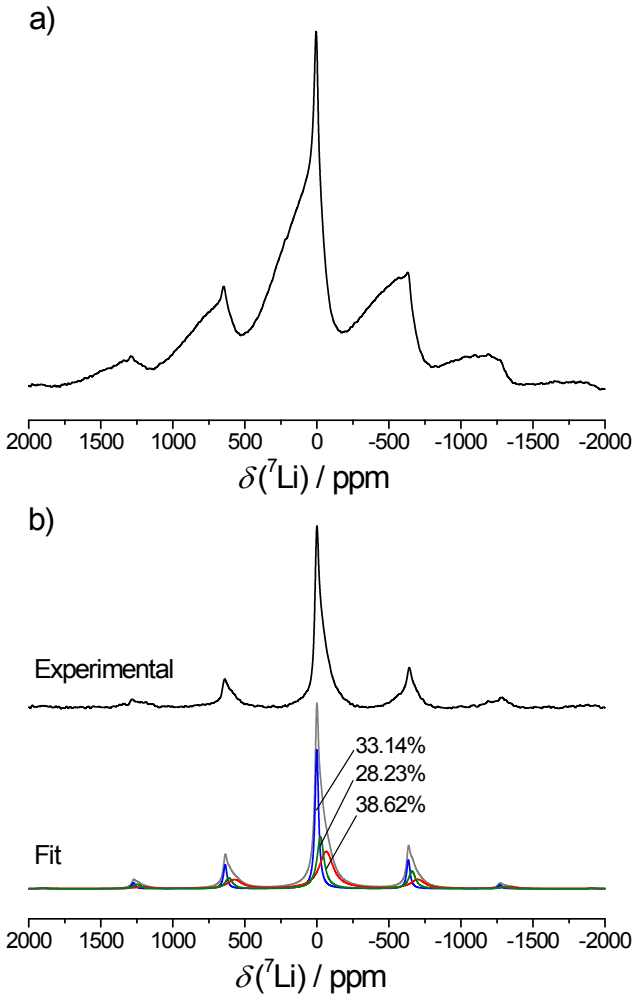

Figure S2. ^{7}Li NMR spectra of the pristine LTMO acquired with Hahn-echo pulse sequence at 2.35 T with MAS frequency of 25 kHz. a) Spectrum acquired with an echo delay of one rotor period exhibiting both P-Li and D-Li signals. b) D-Li signal acquired with an echo delay of two rotor periods in order to filter out the fast-decaying P-Li signal, as the ^{7}Li relaxation is faster in the paramagnetic environment than in the diamagnetic environment due to the interaction with the electron spins around. For the D-Li signal, a similar ^{7}Li line shape with negative shift was observed in the Li_xTiO_2,[2] which could be originated from a Knight shift due to the interaction with conduction band electrons. Three resonances are further identified, corresponding to the Li in Li-rich (0.6 ppm, 33.1%), Li-Ti even distributed (−25 ppm, 28.2%), and Ti-rich (−65 ppm, 38.6%) region, respectively.

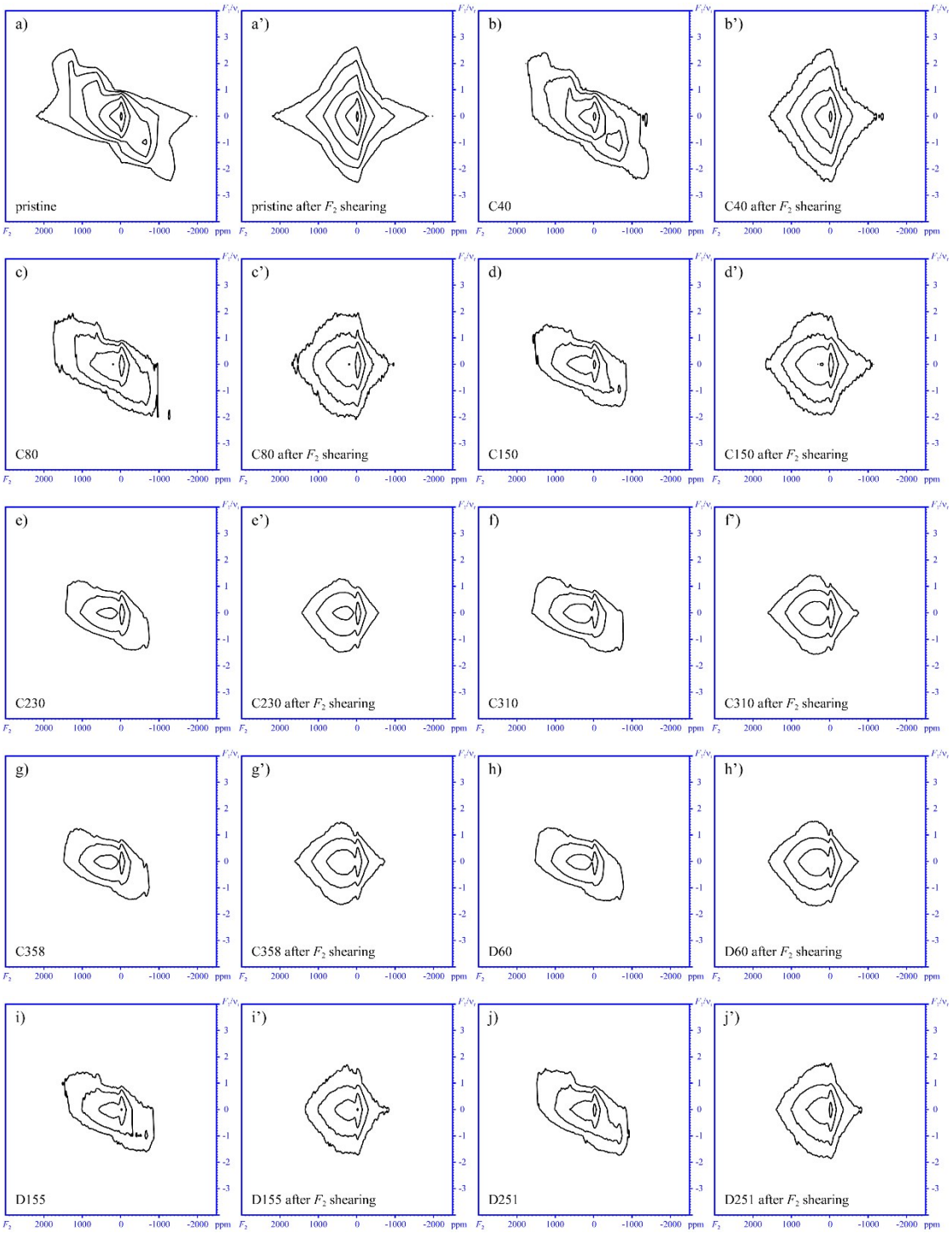

Figure S3. a-j) Pseudo-2D MATPASS spectra of LTMO at different states of charge (SOCs). a'-j') Spectra after F_2 shearing. Isotropic spectra shown in the main article are obtained from summation of each row.

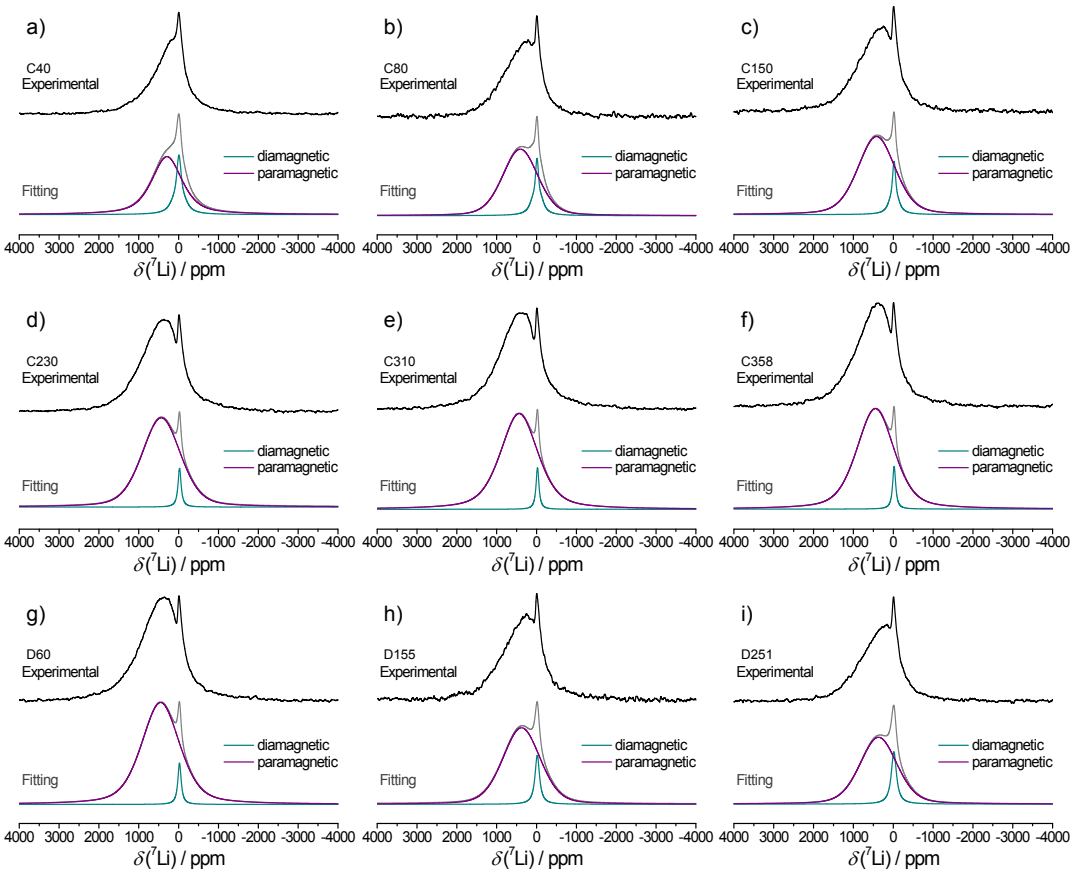

Figure S4. a-i) Deconvolutions of the ex situ ^{7}Li pjMATPASS NMR spectra at different SOCs.

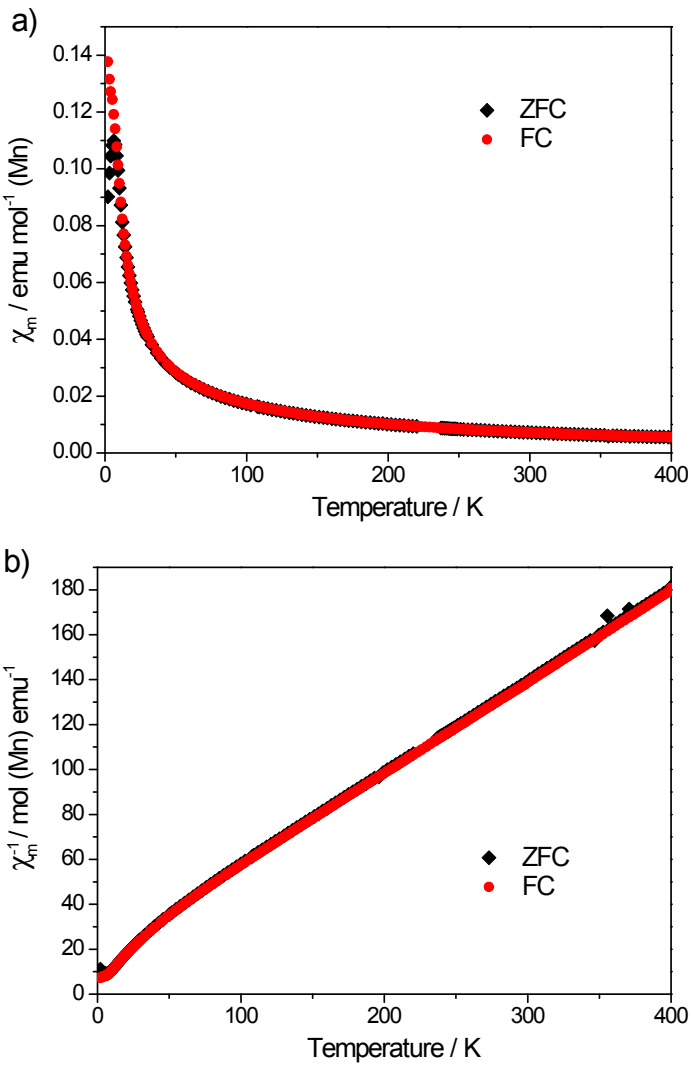

Figure S5. (a) Molar magnetic susceptibility and (b) reciprocal molar magnetic susceptibility of the pristine LTMO measured in a static field of 100 Oe. Linear fitting of the χ_m^{-1} vs. T plot gives the Curie constant (C) of 2.46, which translates into an effective magnetic moment μ_{eff} of 4.44 μ_B since $\mu_{eff} = \sqrt{8C}$. ZFC: zero field cooling. FC: field cooling.

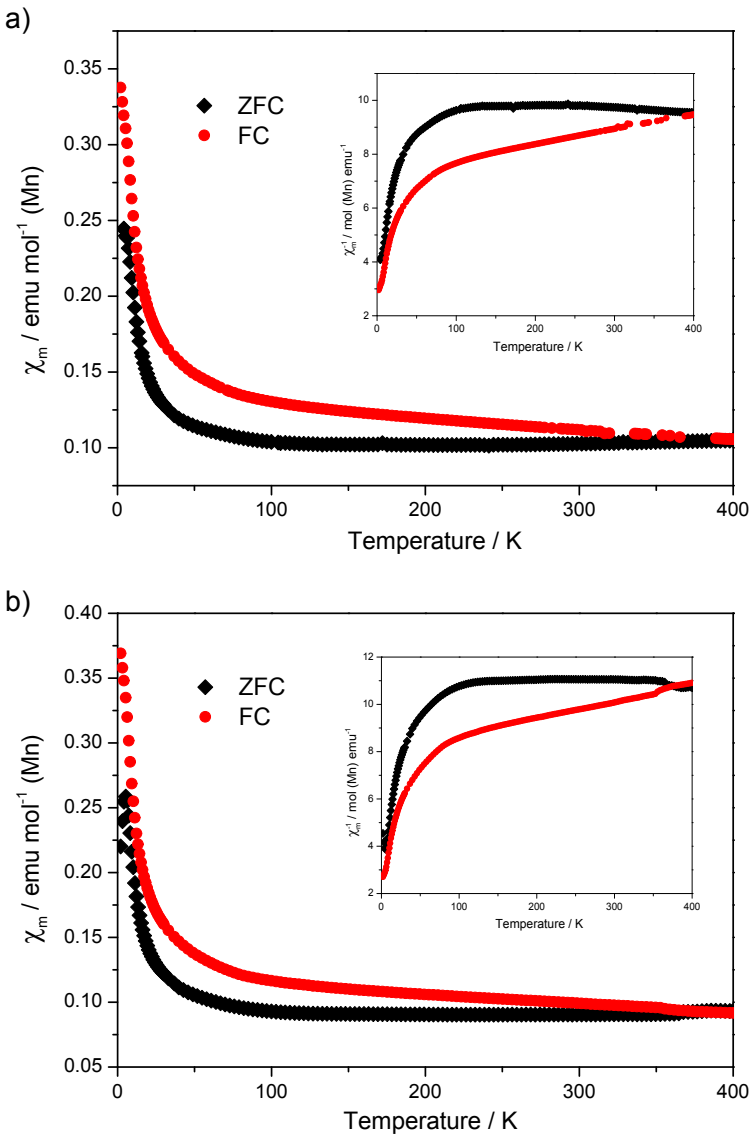

Figure S6. (a) Molar magnetic susceptibility of $Li_{0.8}Ti_{0.4}Mn_{0.4}O_2$ (a) and $Li_{0.4}Ti_{0.4}Mn_{0.4}O_2$ (b), corresponding to the extraction of ca. 1/3 and 2/3 of Li, respectively, measured in a static field of 100 Oe. The inserts show the reciprocal molar magnetic susceptibility of each sample. It is interesting that the molar magnetic susceptibility of these two samples are ca. 12 times larger than that of the pristine sample at room temperature, and a bifurcation between the ZFC and FC magnetization of the charged samples appears below 400 K. These results are consistent with the previous reports on the short-range ferromagnetism,[3,4] which suggests that the ferromagnetic clusters are embedded in nonferromagnetic matrix due to the short-range order. Thus it can be inferred that, in LTMO, the clusters of Mn ions, which become ferromagnetic upon charging, are embedded in the diamagnetic Li and Ti environments.

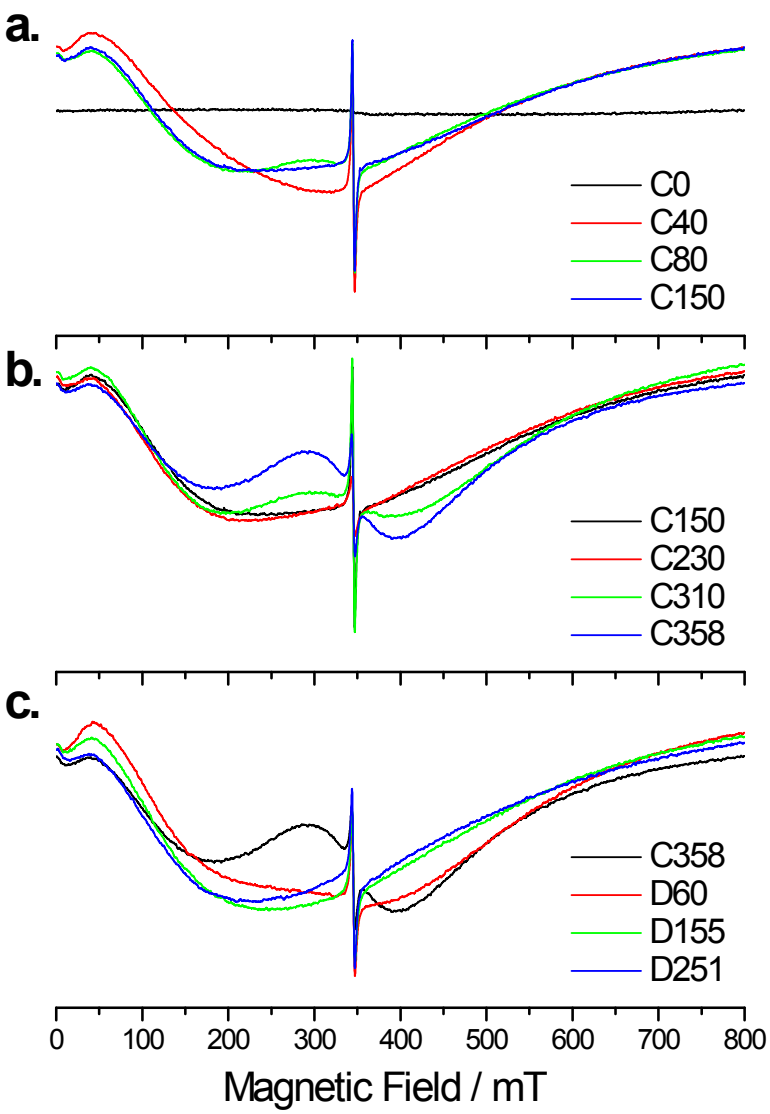

Figure S7. Ex situ room temperature perpendicular-mode CW-EPR spectra of LTMO during the processes of (a) Mn oxidation, (b) O oxidation, and (c) reduction. The sharp signals at ~345 mT result from the delocalized electrons in the Super P conductive additive. The signal of $(O_2)^{n-}$ (n = 1, 2, 3) species is unobservable at room temperature. The Mn^{4+} signals (g ≈ 2.0) for C310 and C358 at room temperature exhibit a narrower Lorentzian line shape as compared to C358 at 1.8 K, as a result of lower ferromagnetic interactions at higher temperature. For the same reason, the Mn^{4+} signal can be observed in C310 at room temperature, indicating the interruption of the Mn^{4+}–O^{2-}–Mn^{4+} superexchange coupling by the formation of electron holes on the oxygen bonded to Mn^{4+}. Furthermore, the more intense Mn^{4+} signal in C358 with respect to C310 indicates the increased amount of the electron holes on the oxygen coordinated by Mn^{4+}.

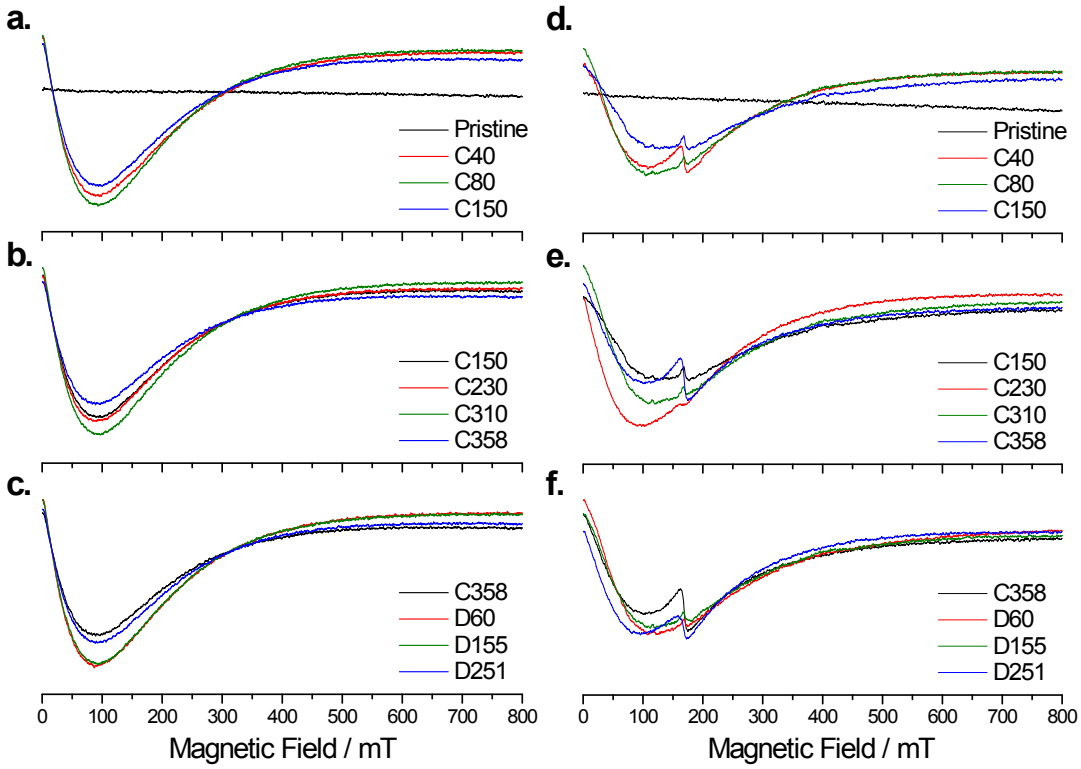

Figure S8. Ex situ parallel-mode CW-EPR spectra of LTMO at different SOCs at room temperature (a–c) and 1.8 K (d–f). Signal intensities are normalized based on the mass of each material scraped from the electrodes. The Mn^{3+} signal in the pristine LTMO is expected to be observed at around 160 mT, but in fact there is no signals observed for the pristine sample at RT and 1.8 K. For the charged samples, the broad signals should be due to the ferromagnetism, in accord with the perpendicular mode data. While there is still no Mn^{3+} signal at RT, the resonances at around 168 mT are observed in the spectra at 1.8 K, but the intensities disagree with the contents of Mn^{3+} in the samples. The unusual resonances may be related to the ferromagnetically coupled spins. The signal intensity at 168 mT becomes exceptionally large for the C358 sample, which may indicate the reduction of the Mn^{4+} to Mn^{3+} during O oxidation by the reductive coupling mechanism.[5] Both of Mn^{3+} and Mn^{4+} are observed in the XAS spectrum of C358 (Figure S12), while only Mn^{4+} is observed in the XPS spectrum (Figure S10). Because the detection depth is much deeper for the XAS technology, this may indicate that the reductive coupling occurs in the bulk but not at the surface.

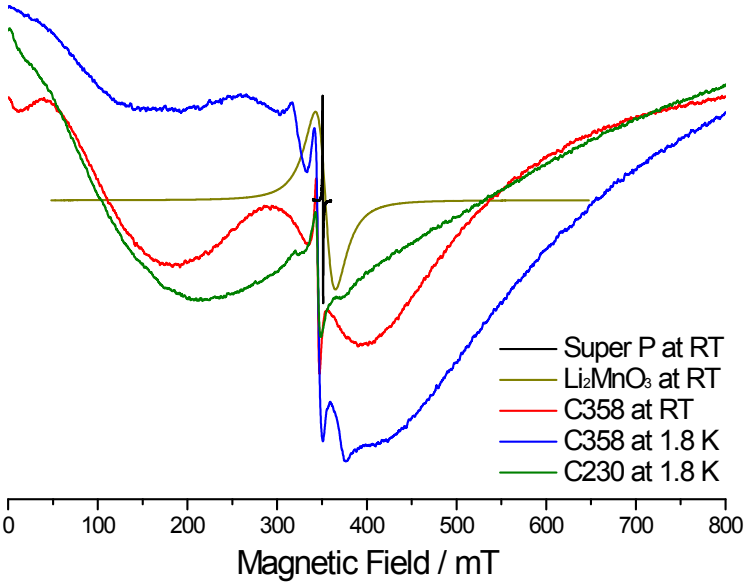

Figure S9. The signals of the charged samples compared to the signals of the raw Super P carbon and Li_2MnO_3. The Mn^{4+} signal is much narrower for Li_2MnO_3 than for C358, and the signal of the raw Super P carbon is much narrower than that in the electrode. The broadening is probably due to the ferromagnetism in the samples, which may also lead to the broadening of the $(O_2)^{n-}$ signals.

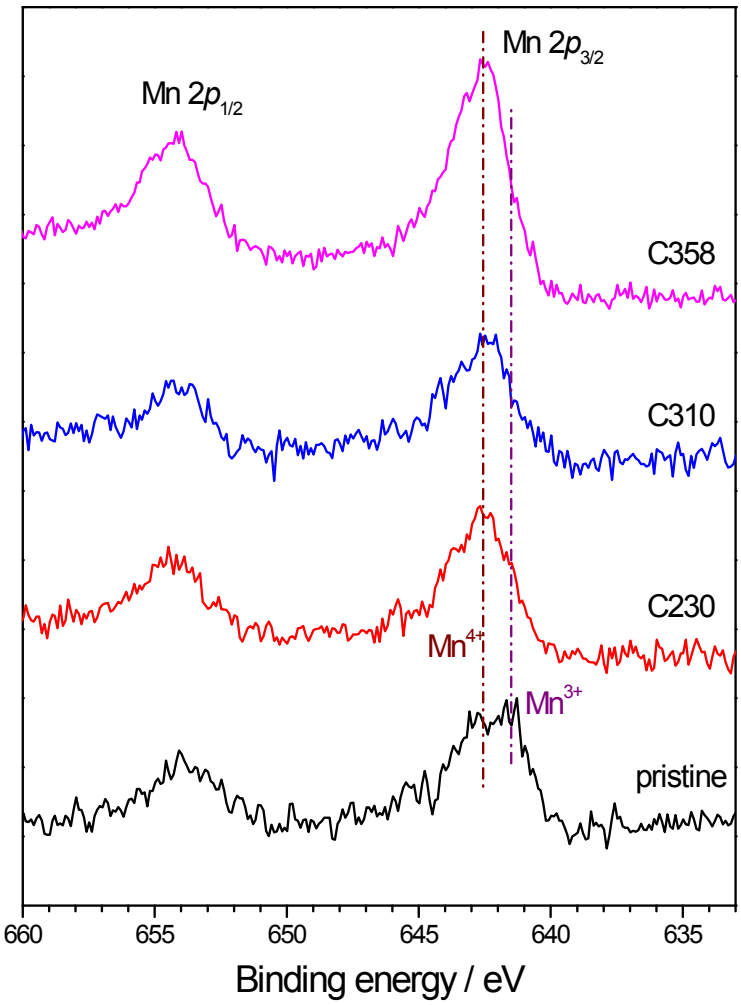

Figure S10. XPS spectra of Mn 2*p* core peaks for the pristine, C230, C310, C358 samples. The Mn $2p_{3/2}$ peaks for C230, C310 and C358 all shift to higher binding energy as compared to the pristine sample, and no peaks can be observed at lower binding energy, indicating that no Mn^{2+} reduced species is formed at the surface of the charged samples.

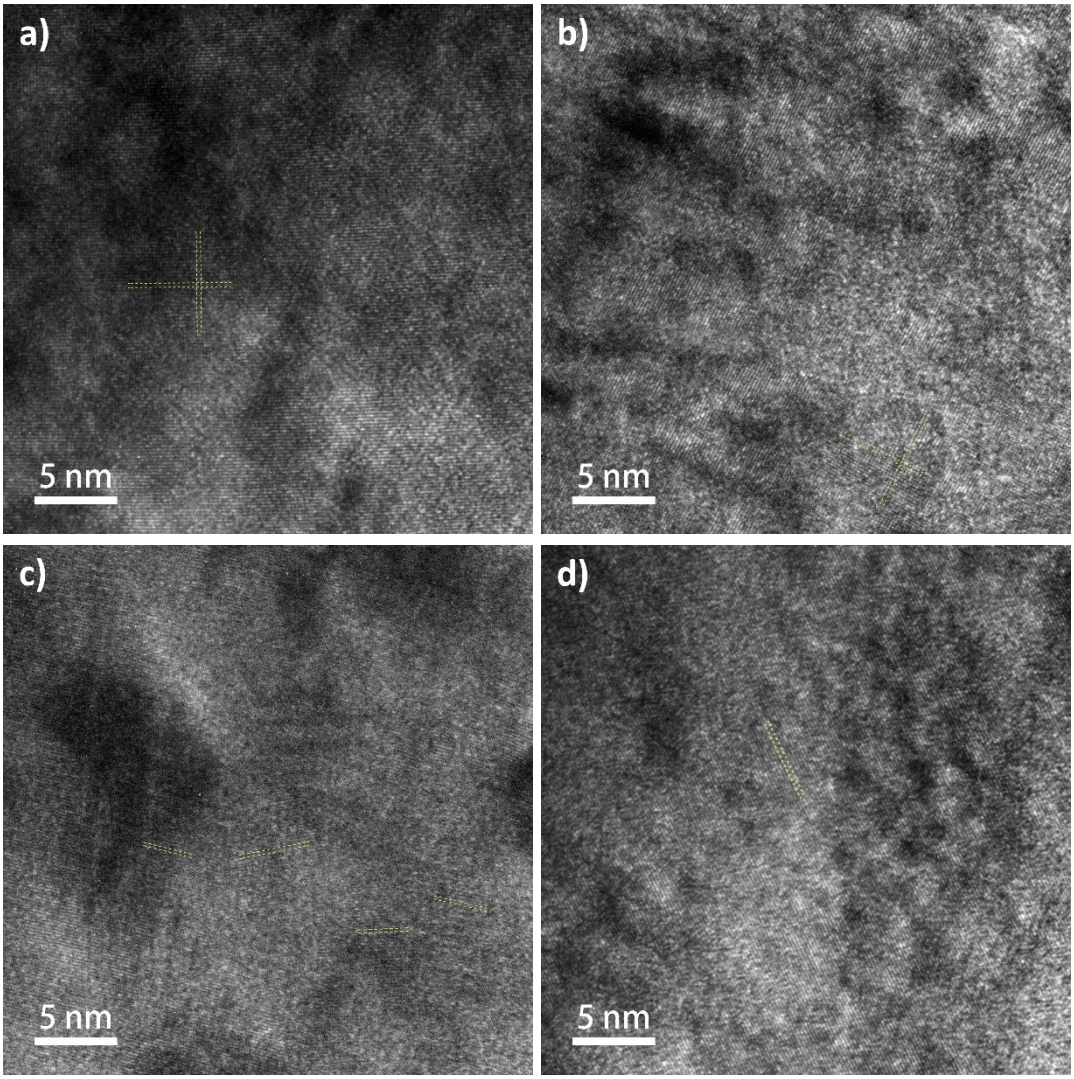

Figure S11. HRTEM images of the pristine sample (a), C150 (b), C358 (c), and D251(d). Dash lines are marked to assist in the recognition of lattice fringes. The d-spacing is measured on the reciprocal lattices to be 0.20375, 0.20059, 0.19887, and 0.20229 nm for the pristine sample, C150, C358, and D251, respectively, in good agreement with the evolution of the lattice parameters of LTMO during cycling.[6]

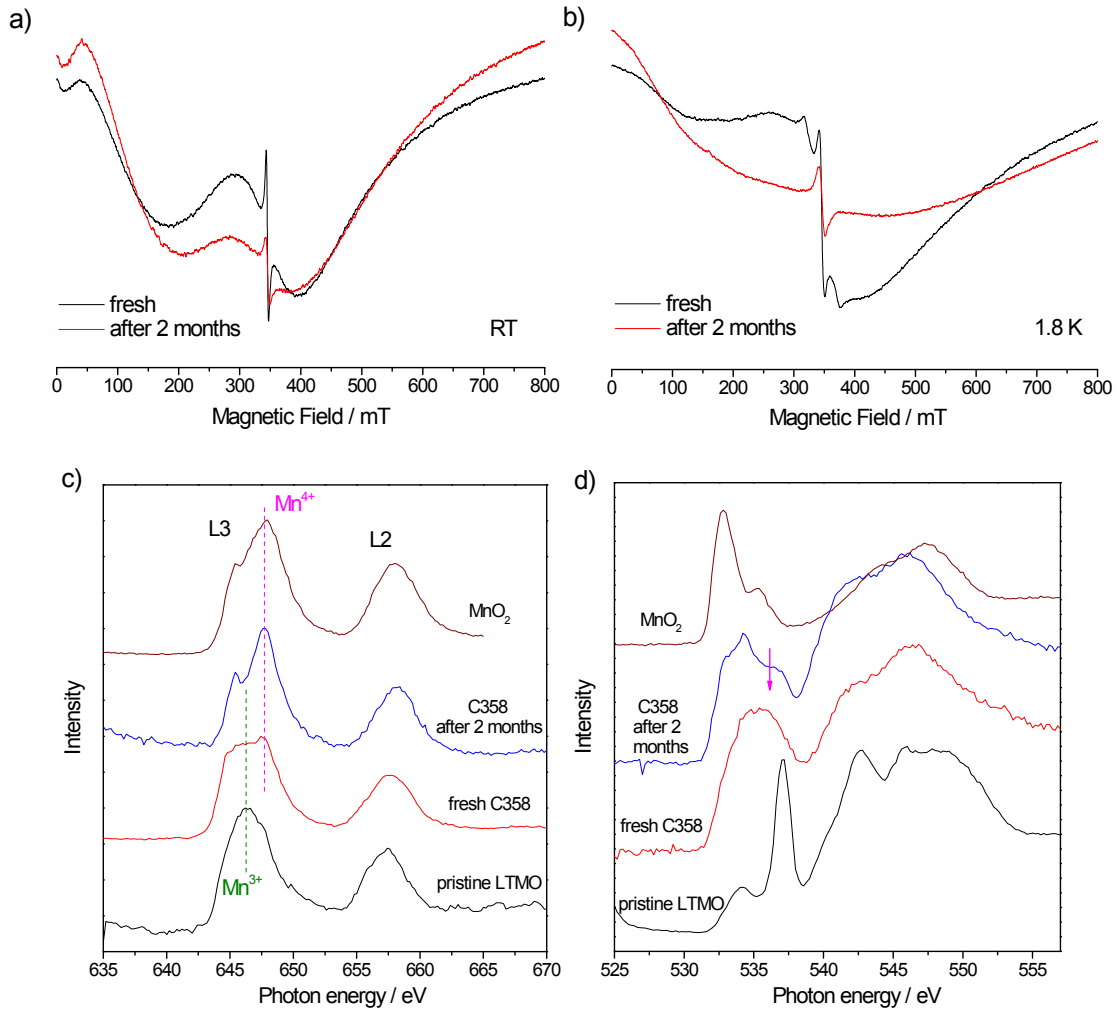

Figure S12. The variation in the electronic structure of the C358 sample being stored in the glove box for 2 months. (a, b) EPR spectra of the fresh C358 and the stored C358 at (a) room temperature and (b) 1.8 K. Mn L-edge (c) and O K-edge (d) XAS profiles of the fresh C358 and the stored C358. As shown in the EPR spectra, after storing in the glove box for 2 months, the Lorentzian line shape for the Mn^{4+} signal decreases at RT and vanishes at 1.8 K, and signal of the electron holes on oxygen disappears at 1.8 K, indicating the rebuilding of the Mn^{4+}–O^{2-}–Mn^{4+} superexchange coupling. Furthermore, the ferromagnetic resonance signal becomes stronger after 2 months. TEY mode sXAS shows the valence change of the Mn ions near the surface. The surface Mn ions in the fresh C358 have a mixed valence of +3 and +4, which is partially reduced due to side reactions with the electrolyte. But after storage in the glove box for 2 months, the Mn valence completely converts to +4. Since there is no extraneous oxidant, it is reasonable to attribute the electron loss to the reduction of lattice oxygen. The pre-edge in the O K-edge SXAS shows the transitions from the O 1*s* to the empty TM 3d orbitals mixed

with O 2*p* orbitals.[7] The density of unoccupied states is reduced, marked by the arrow, suggesting the electron holes are refilled by oxidizing the surface Mn^{3+} ions or the carbon additive.

References:

[S1]C. P. Grey and N. Dupré, *Chem. Rev.*, 2004, **104**, 4493-4512.

[S2]V. Luca, T. L. Hanley, N. K. Roberts and R. F. Howe, *Chem. Mater.*, 1999, **11**, 2089-2102.

[S3]R. Mathieu, P. Nordblad, D. N. H. Nam, N. X. Phuc and N. V. Khiem, *Phys. Rev. B*, 2001, **63**, 174405.

[S4]J. Wu and C. Leighton, *Phys. Rev. B*, 2003, **67**, 174408.

[S5]M. Saubanère, E. McCalla, J. M. Tarascon and M. L. Doublet, *Energy Environ. Sci.*, 2016, **9**, 984-991.

[S6]K. Zhou, S. Zheng, H. Liu, C. Zhang, H. Gao, M. Luo, N. Xu, Y. Xiang, X. Liu, G. Zhong and Y. Yang, *Acs Appl. Mater. Inter.*, 2019, **11**, 45674-45682.

[S7]K. Luo, M. R. Roberts, R. Hao, N. Guerrini, D. M. Pickup, Y. Liu, K. Edström, J. Guo, A. V. Chadwick, L. C. Duda and P. G. Bruce, *Nat. Chem.*, 2016, **8**, 684-691.